

**Prediction of the effect of adsorption on the retention of organic  
compounds by NF/RO using QSPR-ANN**

Nechoua Merarsi <sup>\*1</sup>, Yamina Ammi<sup>1</sup>, and Salah Hanini<sup>1</sup>

<sup>1</sup>Laboratory of Biomaterials and Transport Phenomena (LBMPT),  
University of Medea, Medea 26000, Algeria

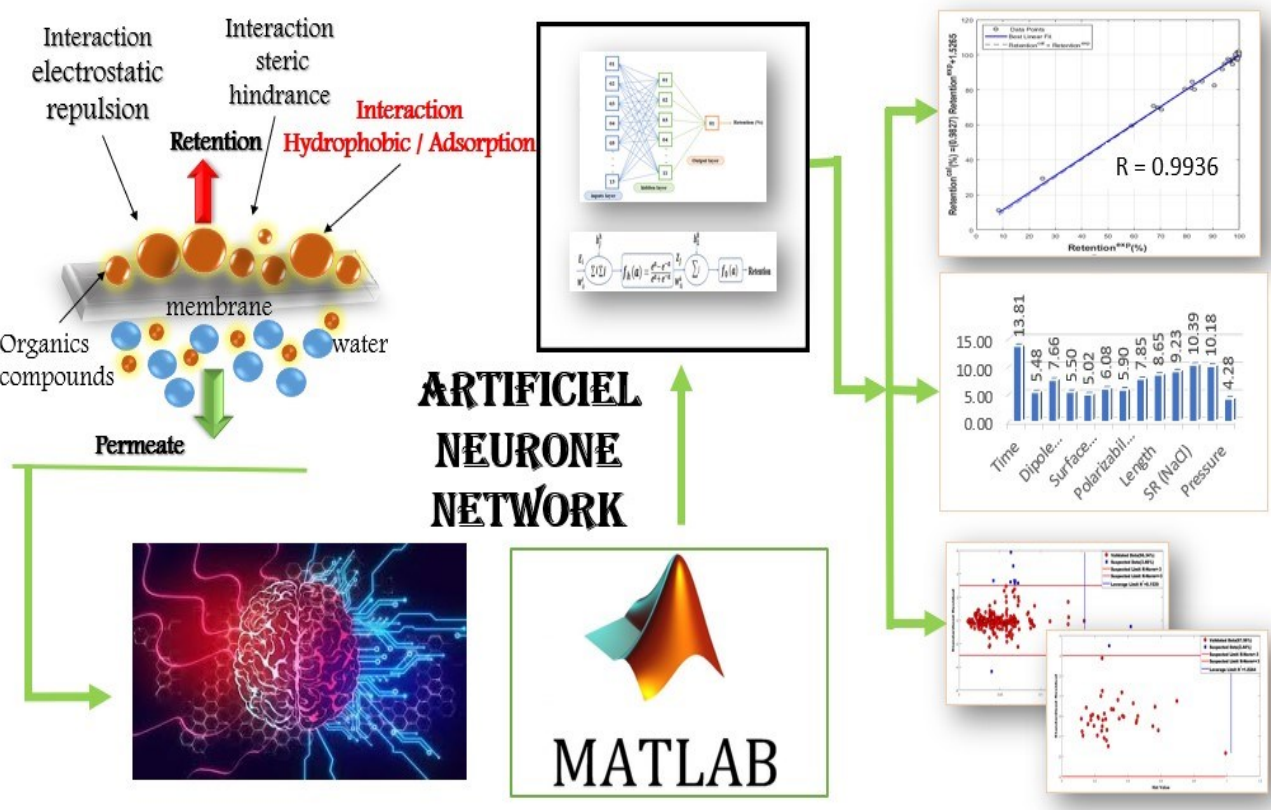
\*Corresponding author: Email: [merarsi.nechoua@gmail.com](mailto:merarsi.nechoua@gmail.com)

[ammi.yamina@yahoo.fr](mailto:ammi.yamina@yahoo.fr)

[s\\_hanini2002@yahoo.fr](mailto:s_hanini2002@yahoo.fr)

Phone number: +213 05 42 72 49 41

39  
40 **Graphical Abstract**



41  
42  
43  
44  
45  
46  
47  
48  
49  
50  
51  
52  
53  
54

## Abstract

Understanding the retention of organic compounds (OCs) is critical for membrane applications in water recycling. The objective of this study was to create an optimized model using Artificial Neural Networks for Quantitative Structure-Property Relationship (QSPR-ANN) to predict the effect of adsorption on the retention of organic compounds (OCs) by nanofiltration (NF) and reverse osmosis (RO).

An optimal model (QSPR-ANN<sub>optimal</sub>) characterized by a similar structure (13 neurons in the inputs layer, 11 neurons in the hidden layer, and 1 neuron in the output layer) is constructed to predict the effect of adsorption on the retention of organic compounds by membranes. A set of 273 data points was used to test the neural network. the data set was used 70% for training, 15% for validation, and 15% for testing. For the most promising neural network model, the calculated retention values were compared to the experimental retention values, and good correlations were found (the determination coefficient " $R^2 = 0.9872$ " and the root mean squared error " $RMSE = 2.2743\%$ " for the test phase). This indicates the good robustness of the established QSPR-ANN model and the possibility of predicting the various parameters that characterize the retention of OCs by RO/NF. Sensitivity analysis revealed that the effect of adsorption retention of organic compounds by reverses osmosis and nanofiltration membranes depends more precisely on two important interactions (hydrophobic/adsorption and steric hindrance).

**Keywords:** Modelisation; hydrophobic adsorption; Interactions; Retention; Organic Compounds; Reverses Osmosis; Nanofiltration; Artificial Neural Networks.

## 1. Introduction

The increasing global utilization of organic compounds (OCs) such as hormones, pesticides, pharmaceuticals, surfactants, and phenolic substances has led to their presence in wastewater effluents, source waters, groundwater, and even treated drinking water. This has given rise to a fresh environmental challenge, prompting significant apprehension among scientists in recent times. Consequently, the removal of OCs has become a subject of great interest. [Dolar et al., \(2013\)](#).

Modern methods are utilized to efficiently eliminate OCs. Among these technologies, membrane processes like RO/NF are particularly good at getting rid of OCs, and protecting the environment and human health. NF/RO methods have previously been shown in several investigations to be capable of eliminating OCs. These investigations have demonstrated a universal relationship between retention efficiency and complex solute-membrane interactions. These interactions include hydrophobic adsorption, electrostatic repulsion, and steric hindrance. The properties of the compounds, such as their hydrophobicity, polarity, molecular size, and charge, as well as the characteristics of the membranes, such as porosity, polarity, and electrostatic charges, affect the interactions between solute-membrane. Furthermore, these interactions are greatly influenced by operational filtration parameters are pressure, pH, permeate flux, temperature, recovery, and cross-flow velocity. [\(Amami et al., 2023; Kim et al., 2018; Teychene et al., 2020\)](#).

[\(Kiso et al., 2001\)](#) The adsorption effect plays a key role in the permeation of solutes in practical water treatment procedures. The extended adsorption and accumulation of solutes on membranes can have a profound influence on the efficacy of solute separation. As per the findings of [\(Comerton et al., 2007\)](#), the initial retention of OCs through membrane adsorption reaches a point of stability when equilibrium is achieved. At this juncture, additional mechanisms, such as electrostatic repulsion and steric hindrance, come into play and contribute to the retention of OCs. Surprisingly, once equilibrium is

reached, adsorption can exert a detrimental impact on retention. Research has demonstrated that adsorbed compounds can dissolve within the active membrane layer, subsequently diffusing through the polymer, and ultimately dissolving on the permeate side of the membrane. Furthermore, when the compound concentration in the feed water drops below the equilibrium value, these molecules adsorb on the permeate side of the NF/RO. For this reason, studying adsorption is crucial to improving our comprehension of membrane retention processes.

A comprehensive understanding of the solute and membrane properties that influence retention forms the basis for a predictive modeling approach to determine the fate of specific compounds in high-pressure membrane applications. Despite numerous research studies attempting to establish connections between the physicochemical properties of solutes and membranes and solute retention, there remains an ongoing need for systematic and comprehensive efforts to identify key parameters that effectively predict solute separation, as well as a concurrent need for a comprehensive understanding of membrane characteristics to predict interactions between OCs and membranes, ultimately influencing retention. as highlighted by (Bellona et al., 2004).

sometimes, real-time analysis can be a time-consuming and laborious task for researchers. Soft computing approaches, such as genetic algorithms, ANN, or fuzzy logic, play an important role in analyzing water engineering problems (water treatment, desalination, and the accurate performance of plants) with minimal space, time, and energy. ANN is a successful soft computing technique that is widely used in chemical engineering research, such as predicting accurate outcomes through appropriate modeling and simulation. It employs a simple mathematical model inspired by the biological analogy of a human brain, it learns from examples of problem datasets and produces meaningful information for performance analysis. It can model and

solve linear, nonlinear, and complex systems (Chan et al., 2023; Mahadeva et al., 2022, 2023).

The literature features a limited quantity of studies attempting to simulate nanofiltration and reverse osmosis processes using artificial neural networks. Nevertheless, only a handful of neural network models exist that can forecast the retention of organic substances in reverse osmosis, forward osmosis, and nanofiltration. (Ammi et al., 2015, 2018, 2020, 2023; Ammi, Khaouane, et al., 2021; Ammi, Hanini, et al., 2021; Khaouane et al., 2017; Kratbi et al., 2023; Libotean et al., 2008; Shahmansouri & Bellona, 2013; Yangali-Quintanilla et al., 2009).

To the best of our knowledge, this marks the initial endeavor in utilizing QSPR-ANN for forecasting the influence of adsorption on the organic compound retention in NF/RO, as well as assessing its predictive capability. Therefore, the present work aims at the prediction of the effect of adsorption on the retention of OCs by NF/RO using QSPR-ANN. The remainder of this study is structured as follows: Section 2: Artificial Neural Networks, section 3: Modeling Procedure, section 4: Results and Discussion, section 5: Sensitivity Analysis, section 6: Applicability Domain, and section 7: Conclusion.

## 2 Artificial Neural Network

Quantitative structure-property relationships (QSPR) is a technique that can predict the properties of chemical/biological systems based on their molecular structure. Relationships are often established using statistical modeling methods, such as artificial neural networks (ANN) Fissa et al., (2023).

Artificial neural networks are powerful tools that are often utilized as black-box models due to their exceptional capacity to learn and generalize nonlinear functional relationships between input and output variables. They operate as data-driven adaptive algorithms, capable of learning from training epochs and uncovering subtle functional correlations within the data, even when the underlying relationships between parameters are ambiguous or challenging to define. With a sufficient amount of data, neural networks can effectively tackle

problems by treating them as multivariate nonlinear statistical models. The connections within neural networks, known as synapses, have adaptive weights that are adjusted during the learning process and are proportional to the synaptic potential. This adaptability allows neural networks to discover complex patterns and relationships in the data, making them valuable for a wide range of applications in fields like machine learning and artificial intelligence [Mohammad et al., \(2022\)](#); [Rehab et al., \(2022\)](#).

The most widely used architecture is Multilayer Perceptron (MLP) with only three layers: 1. The first layer is the input layer, responsible for receiving input data, 2. The middle layer(s), referred to as the hidden layer, processes and passes on the information from the input layer, and 3. The final layer, called the output layer, generates the model's output. The capacity of a neural network to continuously enhance its performance is a fundamental characteristic. With each iteration of the learning process, the network becomes more proficient in understanding and responding to its environment. In the context of neural networks, 'learning' involves the fine-tuning of connection weights, allowing the network to adapt and make increasingly precise predictions and decisions based on the provided data [Mohammad et al., \(2022\)](#); [Rehab et al., \(2022\)](#).

### **3. Modeling procedure**

The modeling procedure involved designing and optimizing the neural network architecture, following the steps outlined in figure 1.

#### **3.1 Data collection, division, pretreatment, and analysis**

In this study, we used available data from 4 references from 2009 to 2018 [Arsuaga et al., \(2010\)](#); [Dolar et al., \(2013, 2017\)](#); [Liu et al., \(2018\)](#). The database contains 273 retention data for 21 OCs (pharmaceutical compounds and phenolics). The list of 21 OCs is presented in the [Supplementary Data \(Table 01\)](#).

The selection of input and output variables is based on the hydrophobic/adsorption interaction between the OCs and the membranes (RO/NF). These interactions between solutes and the

membrane are determined by the descriptors of the OCs, membrane characteristics, and operating conditions Gur-Reznik et al., (2011).

We choose the following inputs:

1 The descriptors of the OCs are molecular weight "Mw", the logarithm of the octanol-water partition coefficient "*log Kow* ", dipole moment, molecular length, surface area min, surface area max, polar surface area, and polarizability;

2 the characteristics of the membranes are molecular weight cut-off "MWCO", sodium chloride salt rejection "SR NaCl", and membrane hydrophobicity "contact angle";

3 the operating condition is pressure.

Molecular descriptors (the MW, the *log Kow*, the polar surface area, and the polarizability) were calculated using ChemSpider ([Http://Www.Chemspider.Com](http://www.chemspider.com), n.d.). We calculated the dipole moment of the descriptor and the molecular size of the descriptor (the molecular length, the surface area min, and the surface area max) by two software (hyperChem and Chembio 3D).

The values of the molecular width, the molecular depth, are defined by the following equations (01,02), and the equivalent molecular width "Eqwidth" was calculated by the following equation (03):

$$Width = \frac{1}{2} \sqrt{S_{\min}} \quad (01)$$

$$Depth = \frac{1}{2} \sqrt{S_{\max}} \quad (02)$$

$$Eqwidth = \sqrt{width * depth} \quad (03)$$

Table 1 displays the minimum (min), maximum (max), mean, and standard deviations (Std) values for both the input and output data.

### 3.2 Model development

The QSAR-ANN models were developed for the prediction of the effect of adsorption on the retention of OCs by (NF) and (RO) membranes. Each neural network contains 23 and 27 variables (13 neurons in the input layer, 9 and 13 neurons in the hidden layer, and 1 neuron in the output layer).



The collective data in this model were randomly divided into two subsets: training and testing; and also, randomly divided into three subsets: training, validation, and testing.

In the process of creating an ANN model, a typical allocation of 60-80% of the data is designated for training, making it the largest segment of the dataset. The training phase signifies the initial step in constructing an ANN model, during which the network learns and establishes the connections between input and output variables. Complex computations occur at this stage, and the neuron weights are adjusted after each epoch using one of the training algorithms to achieve a high level of accuracy. Different criteria, such as the number of epochs or iterations, and a minimum error threshold, can be configured. After the training phase is completed, the remaining data is evenly divided between the validation and testing phases. In the validation phase, the validation dataset which includes unseen data, is utilized to evaluate the predictive capabilities of the ANN model. Employing multiple validation checks helps prevent the model from becoming stuck in local minima. In the testing phase, a distinct set of unseen data is used as input to forecast the output parameters, which assesses the model's performance on new, unseen data [Jawad et al.,\( 2021\)](#).

In this work used the training algorithms are the Regularization-Bayesienne "train-BR" and the Levenberg-Marquard "train-LM". The quantity of neurons in the hidden layer varies based on the network's performance throughout the training phase (9 to 13 neurons). The activation functions used in the hidden layer are the tangent hyperbolic (tansig) and logarithmic sigmoid (logsig) and the activation function used in the output layer is the pure-linear (purelin). The selection of the optimal subset division, the number of hidden neurons, the hidden functions, and the output function (Designing the neural network architecture) for a neural network optimal is done by trial and error method. The prediction of the effect of adsorption on the retention of OCs during NF/RO using QSPR-ANN was performed using MATLAB software.

#### 4. Results and discussion

In this work, QSPR-ANN was used to construct a nonlinear model for the prediction of the effect of adsorption on the retention of OCs by NF/RO membranes. The performance of the model was assessed using the determination coefficient ( $R^2$ ) (values above 0.5 are generally considered satisfactory and values above 0.9 are considered excellent) and the root mean squared error (RMSE) was used to determine the modeling error between the experimental and calculated values, with a perfect RMSE when a Lower value, it is defined as follows [Sediri et al., \(2017\)](#); [Wang et al., \(2009\)](#) :

$$RMSE = \sqrt{\frac{\sum_{i=1}^n (Y_{i,exp} - Y_{i,cal})^2}{n}} \quad (04)$$

with  $n$  is the total number of data points,  $Y_{i,cal}$  represents the calculated values and  $Y_{i,exp}$  is the experimental values from the QSPR-ANN models.

Table 2 shows the RMSE and the  $R^2$  obtained for the effect of adsorption on the retention of OCs by NF/RO under the influence of the training algorithm `trainbr` with the activation function `Tansig` in the hidden layer: division 1 "164 datapoints for the training data (60%) and 109 datapoints for testing data (40%)", division 2 "191 datapoints for the training data (70%) and 82 datapoints for testing data (30%)", and division 3 "218 datapoints for the training data (80%) and 55 datapoints for testing data (20%)" and with training algorithm `trainlm`: division 4 "163 datapoints for training data (60%), 55 datapoints for validation data (20%), and 55 datapoints for testing data (20%)", division 5 "191 datapoints for training (70%), 41datapoint for validation data (15%), and 41 datapoints for testing data (15%)", and division 6 "219 datapoints for training data (80%), 27 datapoints for validation data (20%), and 27 datapoints for the testing data(20%)".

Table 3 shows the RMSE and the  $R^2$  obtained for the effect of adsorption on the retention of OCs by NF/RO under the influence of the activation function "Logsig" in the hidden layer with two training algorithms ("`trainbr`" and "`trainlm`").

The results of the two tables below show that division 5 is the division optimal with the training algorithm Levenberg-Marquard "train-LM" and activation function hyperbolic tangent sigmoid "Tansig". The QSPR-ANN5 model with the structure optimal (train-LM and activation function Tansig) gives lower errors than the other models (RMSE = 2.2743 and R2 = 0.9872 for the testing phase). We conclude the superiority of the optimal neural networks (QSPR-ANN<sub>5</sub>) for modeling the effect of adsorption on the retention of OCs by NF/RO.

The structure of the optimized QSPR-ANN for the prediction of the effect of adsorption on the retention of OCs by NF/RO is cited in figure2, and a more detailed illustration of its architecture is in table 4.

The weight matrices and bias vectors of the QSPR-ANN<sub>optimal</sub> model are listed in [Supplementary Data \(Table 02\)](#).

indices  $w_{ji}^l$  is the input-hidden layer connection weight matrix (11 rows  $\times$  13 columns),

$b_j^h$  is the hidden neurons bias column vector (11 rows),

$w_{1,j}^h$  is the hidden layer-output connection weight matrix (11 rows  $\times$  1 column),  $b_1^0$  is the output neurons bias column vector (1 row).

From the optimized QSPR-ANN<sub>optimal</sub>, assimilation of the effect of adsorption on the retention of OCs by the NF/RO be expressed by a mathematical model that incorporates all the inputs  $E_i$  (time, molecular weight "Mw", dipole moment, surface area min, surface area max, polar surface area, polarizability,  $\log K_{ow}$ , length, MWCO, SR(NaCl), contact angle, and pressure).

The instance outputs  $Z_j$  of the hidden layer:

$$Z_j = f_h \left[ \sum_{i=1}^{13} w_{ji}^l E_i + b_j^h \right] = \frac{\exp \left( \sum_{i=1}^{13} w_{ji}^l E_i + b_j^h \right) - \exp \left( - \sum_{i=1}^{13} w_{ji}^l E_i + b_j^h \right)}{\exp \left( \sum_{i=1}^{13} w_{ji}^l E_i + b_j^h \right) + \exp \left( - \sum_{i=1}^{13} w_{ji}^l E_i + b_j^h \right)} \quad (05)$$

$j = 1, 2, 3, \dots, 11$

The output "Retention":

$$\text{Retention} = f_o \left[ \sum_{j=1}^{11} w_{1,j}^h Z_j + b_1^0 \right] = \sum_{j=1}^{11} w_{1,j}^h Z_j + b_1^0 \quad (06)$$

The combined equations (05) and (06) lead to the following mathematical formula, which describes the retention assimilation by considering all indices  $E_i$ :

$$\begin{aligned} &\text{Retention} \\ &= \sum_{j=1}^{11} w_{1,j}^h \frac{\exp(\sum_{i=1}^{13} w_{ji}^l E_i + b_j^h) - \exp(-\sum_{i=1}^{13} w_{ji}^l E_i + b_j^h)}{\exp(\sum_{i=1}^{13} w_{ji}^l E_i + b_j^h) - \exp(-\sum_{i=1}^{13} w_{ji}^l E_i + b_j^h)} \\ &+ b_1^0 \end{aligned} \quad (07)$$

The linear regression's parameters and plot are easily generated with the MATLAB function "postreg" (Figure 3 (a), (b), (c), and (d)). The comparison of the estimated retention values calculated by the QSPR-ANN model with the experimental retention values reveals great agreement between them, with agreed vectors getting closer to the ideal " $\alpha=1$  (the slope),  $\beta=0$  (y-intercept), and  $R=1$  (correlation coefficient)":  $[\alpha, \beta, R] = [0.9780, 1.7480, 0.9872]$  for the total phase,  $[\alpha, \beta, R] = [0.9776, 1.5560, 0.9854]$  for the training phase,  $[\alpha, \beta, R] = [0.9756, 1.0152, 0.9901]$  for the validation phase, and  $[0.9827, 1.5265, 0.9936]$  for the testing phase respectively.

The errors of the QSPR -ANN optimal for the total phase, the training phase, the validation phase, and the testing phase were calculated to confirm the prediction for the effect of adsorption on the retention of OCs by NF and RO membranes.

The root mean squared error (RMSE), the errors are the mean absolute error (MAE), the standard error of prediction (SEP), residual predictive deviation (RPD), range error ratio (RER), the mean square error (MSE), the mean relative squared error (MRSE), the accuracy factor (Af), and bias factor (Bf).

The error values were obtained with the following equations [Dahmani et al., \(2022\)](#):

$$MAE = \frac{1}{n} \sum_{i=1}^n |(y_{i,exp} - y_{i,cal})| \quad (08)$$

$$SEP(\%) = \frac{RMSE}{y_e} \times 100 \quad (09)$$

$$RPD = \frac{SD}{RMSE} \quad (10)$$

$$RER = \frac{max - min}{RMSE} \quad (11)$$

$$MSE = \frac{1}{n} \sum_{i=1}^n (y_{i,exp} - y_{i,cal})^2 \quad (12)$$

$$MRSE = \frac{1}{n} \sum_{i=1}^n \left( \frac{y_{i,exp} - y_{i,cal}}{y_{i,exp}} \right)^2 \quad (13)$$

$$A_f = \frac{1}{n} \sum_{i=1}^n \left| \log \frac{y_{i,cal}}{y_{i,exp}} \right| \quad (14)$$

$$B_f = \frac{1}{n} \sum_{i=1}^n \left( \log \frac{y_{i,cal}}{y_{i,exp}} \right) \quad (15)$$

where n: the total number of data points,

$Y_{i,exp}$ : the experimental retention value,

$Y_{i,cal}$  : the calculated retention value,

$Y_e$ : the mean value of experimental data,

SD: the standard deviation of experimental data,

min: the minimum of experimental data,

max: the maximum of experimental data.

Table 5 represents the statistical parameters of the QSPR-ANN optimal model. The determination coefficient ( $R^2$ ) in both the training and validation phases is quite high, with values of 0.9710 and 0.9803, respectively, indicating excellent agreement between the experimental and calculated results. The determination coefficient ( $R^2$ ) for the testing phase measures the model's ability to interpolate, and it's impressively high at 0.9872, demonstrating a strong match between experimental and calculated retention. On the flip side, we have embraced the five-level interpretations of Residual Predictive Deviation "RPD" and Range Error Ratio "RER" provided by [Viscarra Rossel et al., \(2006\)](#): excellent predictions (RPD and RER > 2.5); good predictions (RPD and RER of

2.0 to 2.5); approximate quantitative predictions (RPD and RER of 1.8 to 2.0); the ability to distinguish between high and low values (RPD and RER of 1.4 to 1.8); and unsuccessful predictions (RPD and RER < 1.40) [Amami et al., \(2020; Viscarra Rossel et al., \(2006\)\)](#).

The RPD = 628.1936 (%) and RER = 28.5923 (%) values of the QSPR-ANNoptimal model are notably higher than 2.5 for the total phase. Furthermore, various other statistical parameters, including MAE, SEP, MSE, MRSE, Af, and Bf, reinforce the model's strong predictive power across the total, training, validation, and testing phases. These results collectively highlight the model's ability to capture the nonlinear relationship between adsorption effects and the retention of OCs by NF/RO.

## 5. Sensitivity analysis

The analysis of the QSPR-ANNoptimal model establishes the relationship between inputs and outputs. To see the contribution as well as the variation profile of each input variable (time, molecular weight "Mw", dipole moment, surface area min, surface area max, polar surface area, polarizability, *logK<sub>ow</sub>*, length, MWCO, SR(NaCl), contact angle, and pressure) on the output (retention), sensitivity analysis is often used to study how inputs affect outputs [Baghban et al., \(2017\)](#). A "weight" method sensitivity analysis was performed. The method was first proposed by Garson (1991) and repeated by Goh (1995) [Gevrey et al., \(2003\)](#). The process of calculating the importance of "weights" is grounded in the following equation, as outlined in the research conducted by [Dahmani et al., \(2022\)](#):

$$\text{IR (relative importance)} = \frac{\text{Connection Weights of Input-Hidden}}{\text{Connection Weights of Hidden-Output}}$$

This equation provides a measure of the relative importance of the connection weights between the input and hidden layers compared to the connection weights between the hidden and output layers within the neural network.

$$RI_i (\%) = 100 * \frac{\sum_{j=1}^{n_j} \frac{|w^I * W^H|}{\sum_{i=1}^{n_i} |w^I * W^H|}}{\sum_{i=1}^{n_i} \sum_{j=1}^{n_j} \frac{|w^I * W^H|}{\sum_{i=1}^{n_i} |w^I * W^H|}} \quad (16)$$

The results of the contributions are presented in figure 4. The most relevant variables (RI> 5%) that can influence for prediction of the effect of adsorption on the retention of OCs by RO/NF membranes are time, MW, dipole moment, surface area min, surface area max, polar surface area, polarizability, *logKow*, length, MWCO, SR(NaCl), and contact angle.

Figure 4 shows that the retention of OCs by reverse osmosis and nanofiltration is governed by two important interactions (hydrophobic/adsorption interaction and steric hindrance "sieving effect"). The first interaction (hydrophobic/adsorption) takes place between hydrophobicity/polarity of OCs "*logKow* (IR=7.85%), dipole moment (IR = 7.66%), polar surface area (IR = 6.08%), and polarizability (IR = 5.90%)" and hydrophobicity/polarity of membranes "contact angle (IR = 10.18%)". The second interaction steric hindrance "sieving effect" occurs between the parameter steric / size of OCs "length (IR = 7.85%), surface area min (IR = 5.50%), MW (IR = 5.48%), surface area max (IR = 5.02%)" and the parameter steric / size of membrane " MWCO (IR = 9.23%) and SR(NaCl) (IR = 10.38%)". This research work suggests that the OCs retention on the NF/RO strongly depends much more on the time (IR = 13.21%), SR(NaCl), and contact angle.

It is clear that steric/size SR (NaCl) is more suitable for modeling the impact of adsorption on the retention of OCs by RO/NF compared to steric/size MWCO (molecular weight cutoff) (RI (MWCO) = 9.23% and RI (SR "NaCl") = 10.38%). Consequently, characterizing a membrane in terms of the steric/size SR (NaCl) parameter is a simpler and more appropriate approach than using MWCO. These findings align with the results from previous studies by Ammi et al., (2020).

The sensitivity analysis using the weight method has effectively determined the true significance of all the variables employed in

predicting the impact of adsorption on the retention of OCs by RO/NF. This, in turn, validates the appropriateness of the selected variables utilized in this research study.

## 6. Applicability domain

The accuracy with which data points are identified has a significant impact on the validity of the model [Peter J. Rousseeuw, \(2005\)](#) . Note that, as previously mentioned, this study used a database, these data points may potentially include errors stemming from laboratory measurements. Outliers are data points that deviate from the general trend of the main data points. therefore, it is important to employ robust outlier detection methods to identify and exclude imprecise experimental data, ultimately enhancing the accuracy of the model. [Hosseinzadeh & Hemmati-Sarapardeh, \(2014\); Mohammadi et al., \(2012\)](#) . Corresponding methods often include numerical and graphical algorithms [Peter J. Rousseeuw, \(2005\)](#) . In this study, we use the mathematical method of leverage to find outliers. The method first computes the residuals and then creates a hat matrix from the input data points according to [Moammadi et al., \(2012\); Peter J. Rousseeuw, \(2005\)](#):

$$H = X(X^tX)^{-1}X^t \quad (17)$$

Here, X denotes a matrix of dimensions  $m \times n$ , where n corresponds to the number of inputs layer (rows), m is the model parameters (columns), and t represents the transpose matrix. The Hat values of the data are derived from the main diagonal of the matrix H.

$$Hat = diagonal(H) \quad (18)$$

the Williams plot is created to visually detect suspended data or outliers. The plot illustrates the correlation between Hat indices and standardized cross-validated residuals. These residuals are calculated as the variance between the represented or predicted values and the implemented data.

$$H^* = \frac{3(n+1)}{m} \quad (19)$$



A leverage value ( $H^*$ ) of three is typically regarded as a 'cut-off' point, accepting points within a range of  $\pm 3$  standard deviations from the mean (bounded by two horizontal red lines) to encompass 99% of normally distributed data [Baghban et al., \(2017\)](#); [Hosseinzadeh & Hemmati-Sarapardeh, \(2014\)](#); [Mohammadi et al., \(2012\)](#).

the standardized cross-validated residuals are calculated from the data of the retention experimental and that calculated by the model

$$(R\_Norm)_i = \frac{(Retention_i^{exp} - Retention_i^{cal})}{\sqrt{var(Retention_i^{exp} - Retention_i^{cal})}}, \quad i = 1, \dots, m \quad (20)$$

If the majority of the data points fall within the ranges of  $0 \leq \text{Hat} \leq H^*$  and of  $-3 \leq R\_Norm \leq 3$  it indicates that the model development and its predictions occur within the domain of applicability, which leads to a model statistically valid. Thus, we can identify "Good High Leverage" points in the domain of  $0 \leq \text{Hat} \leq H^*$  and  $-3 \leq R\_Norm \leq 3$ . However, points falling outside this range, with  $R\_Norm < -3$  or  $R\_Norm > 3$  (whether greater or less than the  $H^*$  value) are classified as model outliers or as "Bad High Leverage" points [Baghban et al., \(2017\)](#); [Hosseinzadeh & Hemmati-Sarapardeh, \(2014\)](#); [Mohammadi et al., \(2012\)](#).

Figure 5 represents Williams range plot of QSPR-ANN optimal neural model for the total phase. This plot contains 263/273 (96.34%) validated data points (red) and 10/273 (3.66%) suspected data points (blue). The critical leverage value is  $H^* = \frac{3(n+1)}{m} = \frac{3(13+1)}{273} = 0.1539$ .

This indicates that the development of the optimal QSPR-ANN model and its prediction are within bounds leading to the optimal statistically valid neural model. Therefore, we can affirm that there are "Good Haut Levier" points for the total phase.

Figure 6 represents Williams range plot of QSPR-ANN optimal neural model for testing phase. This plot contains 40/41 (97.56%) validated data points (red) and the blue line vertically and 1/41 (2.44%) suspected data points (blue). The critical leverage value is  $H^* = \frac{3(n+1)}{m} =$

$\frac{3(13+1)}{41} = 1.0244$  . This indicates that the development of the optimal QSPR-ANN model and its prediction are within bounds leading to the optimal statistically valid neural model. Therefore, we can affirm that there are "Good Haut Levier" points for the test phase.

## 7. Conclusion

The present paper demonstrates the use of the QSPR-ANN<sub>optimal</sub> which was developed to predict the effect of adsorption on the retention of OCs by nanofiltration and reverse osmosis. The QSPR-ANN optimal can summarize interactions between the descriptors of OCs are Mw, *log Kow*, dipole moment, molecular length, surface area min, surface area max, polar surface area, and polarizability, the characteristics of the membranes are MWCO, SR NaCl, and contact angle, and the operating conditions is pressure.

An optimal QSPR-ANN is characterized by a structure (13 neurons in the input layer, 11 neurons in the hidden layer, and 1 neuron in the output layer). Training algorithm Levenberg-Marquard "train- LM" with activation function "Tansig " in the hidden layer and "Purlin" in the output layer. QSPR-ANN<sub>optimal</sub> showed good agreement between calculated and experimental data by the testing phase, with a coefficient of determination " $R^2 = 0.9872$ " and a root mean square error "RMSE = 2.2743%".

The sensitivity analysis conducted through the weight method successfully identified the true importance of all the utilized variables for the prediction of the effect of adsorption on the retention of OCs by RO/NF which is governed by two important interactions (hydrophobic/adsorption interaction and steric hindrance "sieving effect"), As a result, proves the correctness of the choice of variables appropriateness that were used in this study. The SR(NaCl) may be a possible lump parameter for the prediction of the effect of adsorption on the retention of OCs by NF/RO.

Applicability domain and Diagnostic analysis of the outliers of the optimized neural model (QSPR ANN optimal) demonstrated that both its development and its predictions are performed in the application

domain. This substantiates the statistical validity optimal neural model.  
 indicating the presence of "Good High Leverage" points during the test  
 phase.

#### Abbreviation

<b>OCs</b>	Organic Compounds,
<b>QSPR</b>	Quantitative Structure-Property Relationships,
<b>ANN</b>	Artificial Neural Networks,
<b>RO</b>	Reverse Osmosis,
<b>NF</b>	Nanofiltration,
<b>MLPs</b>	Multilayer Perceptron,
<b>Mw</b>	molecular weight,
<b><i>log Kow</i></b>	logarithm of the octanol-water partition coefficient,
<b>MWCO</b>	molecular weight cut-off,
<b>SR NaCl</b>	sodium chloride salt rejection,
<b>S<sub>min</sub></b>	surface area min
<b>S<sub>max</sub></b>	surface area max
<b>Min</b>	minimum,
<b>Max</b>	maximum,
<b>Mean</b>	means,
<b>Std</b>	standard deviations,
<b>RMSE</b>	root mean squared error,
<b>R<sup>2</sup></b>	determination coefficient,
<b>train-BR</b>	Regularization-Bayesienne,
<b>train-LM</b>	Levenberg-Marquard,
<b>tansig</b>	tangent hyperbolic,
<b>logsig</b>	logarithmic sigmoid,
<b>purelin</b>	pure-linear,
<b>MAE</b>	mean absolute error,
<b>MPE</b>	model predictive error,
<b>SEP</b>	the standard error of prediction,
<b>RPD</b>	residual predictive deviation,

593	<b>RER</b>	range error ratio,
594	<b>MSE</b>	the mean square error,
595	<b>MRSE</b>	the mean relative squared error,
596	<b>Af</b>	the accuracy factor,
597	<b>Bf</b>	bias factor,
598	<b>IR</b>	relative importance,
599	<b>Exp</b>	experimental,
600	<b>Cal</b>	calculated,
601	<b>W</b>	weights,
602	<b>b</b>	bais.

#### Acknowledgements

The authors gratefully acknowledge the Ministry of Higher Education of Algeria (PRFU Projects N°A16N01UN260120220004) and the group of Laboratory of Biomaterials and Transport Phenomena in the University of Medea for their help throughout this project.

## Tables.

**Table 1.** Statistical analysis of inputs and output.

	Min	Max	Mean	Std
<b>Temps (h)</b>	0.0000	24.0000	6.5616	7.1859
<b>MW (g mol<sup>-1</sup>)</b>	94.1100	392.4700	288.0913	70.4984
<b>Dipole moment (Debye)</b>	0.2358	6.3000	4.0203	1.4071
<b>Log K<sub>ow</sub></b>	-1.2200	3.4800	1.7275	0.9046
<b>Polar Surface Area (nm<sup>2</sup>)</b>	0.2000	1.3000	0.7592	0.2732
<b>Polarizability (nm<sup>3</sup>)</b>	0.0112	0.0397	0.0311	0.0065
<b>Length (nm)</b>	0.0970	0.1719	0.1472	0.0146
<b>Surface area min (nm<sup>2</sup>)</b>	2.1394	5.1640	4.1329	0.6206
<b>Surface area max (nm<sup>2</sup>)</b>	2.4437	7.8549	5.3434	1.2226
<b>MWCO (Dalton)</b>	100.0000	340.0000	185.9341	102.0720
<b>SR (CaCl<sub>2</sub>) (%)</b>	-	-	-	-
<b>SR(NaCl) (%)</b>	20.5300	98.6400	73.9201	23.4504
<b>Contact angle (°)</b>	20.1000	73.1600	53.5681	14.3834
<b>Pressure (KPa)</b>	1000.0000	4100.0000	1127.4725	523.1549
<b>Retention (%)</b>	7.1713	100.0000	86.0097	20.3951

648  
649  
650

**Table 2.** Effect of dividing the database with the activation function (tansig) and two training algorithms.

Splitting the database into two subsets (trainbr)				Splitting the database into three subsets (trainlm)			
		R <sup>2</sup>	RMSE (%)			R <sup>2</sup>	RMSE (%)
Division 01	Total phase 100%: 273 datapoints	0.9720	3.4079	Division 04	Total phase 100%: 273 datapoints	0.9575	4.1991
	Training phase 60%: 164 datapoints	0.9986	0.7735		Training phase 60%: 163 datapoints	0.9732	3.2192
	Validation phase	-	-		Validation phase 20%: 55 datapoints	0.9306	5.1949
	Test phase 40%: 109 datapoints	0.9283	5.3092		Test phase 20%: 55 datapoints	0.9458	5.4609
Division 02	Total phase 100%: 273 datapoints	0.9779	3.0317	Division 05	Total phase 100%: 273 datapoints	0.9746	3.2466
	Training phase 70%: 191datapoints	0.9892	2.1833		Training phase 70%: 191datapoints	0.9710	3.4460
	Validation phase	-	-		Validation phase 15%: 41 datapoints	0.9803	3.1136
	Test phase 30% :82 datapoints	0.9428	4.4154		Test phase 15%: 41 data points	0.9872	2.2743
Division 03	Total phase 100%: 273 datapoints	0.9843	2.5813	Division 06	Total phase 100%: 273 datapoints	0.9817	2.7565
	Training phase 80%: 218 datapoints	0.9976	1.0165		Training phase 80%: 219datapoints	0.9880	2.1326
	Validation phase	-	-		Validation phase 10%: 27 datapoints	0.9752	3.6410
	Test phase 20%: 55 datapoints	0.9368	5.3830		Test phase 10%: 27 datapoints	0.9553	5.1654

651  
652  
653  
654  
655  
656  
657  
658  
659  
660  
661  
662  
663  
664

**Table 3.** Effect of dividing the database with the activation function (logsig) and two training algorithms.

Splitting the database into two subsets (trainbr)				Splitting the database into three subsets (trainlm)			
		R <sup>2</sup>	RMSE (%)			R <sup>2</sup>	RMSE (%)
Division 01	Total phase 100%: 273 datapoints	0.9706	3.5450	Division 04	Total phase 100%: 273 datapoints	0.9584	4.1779
	Training phase 60%: 164 datapoints	0.9872	2.2732		Training phase 60%: 163 datapoints	0.9912	1.9056
	Validation phase	-	-		Validation phase 20%: 55 datapoints	0.9122	6.2009
	Test phase 40%: 109 datapoints	0.9504	4.8684		Test phase 20%: 55 datapoints	0.9071	6.1179
Division 02	Total phase 100%: 273 datapoints	0.9783	3.0157	Division 05	Total phase 100%: 273 datapoints	0.9631	3.9284
	Training phase 70%: 191 datapoints	0.9874	2.3662		Training phase 70%: 191 datapoints	0.9890	2.2767
	Validation phase	-	-		Validation phase 15%: 41 datapoints	0.8290	5.8909
	Test phase 30% :82 datapoints	0.9532	4.1518		Test phase 15%: 41 data points	0.8894	6.6263
Division 03	Total phase 100%: 273 datapoints	0.9888	2.1525	Division 06	Total phase 100%: 273 datapoints	0.9549	4.3426
	Training phase 80%: 218 datapoints	0.9918	1.8637		Training phase 80%: 219 datapoints	0.9626	3.9661
	Validation phase	-	-		Validation phase 10%: 27 datapoints	0.9586	5.3357
	Test phase 20%: 55 datapoints	0.9791	3.0381		Test phase 10%: 27 datapoints	0.8327	5.8836

677

**Table 4.** Structures of the optimized QSPR-ANN model.

Training Algorithm	Input layer	Hidden layer		Output layer	
	Neurons numbers	Neurons numbers	Activation function	Neurons numbers	Activation function
Levenberg-Marquard "LM"	13	11	tansig	1	purelin

678

679

680

681

682

683

684

685

686

687

688

689

690

691

692

693

694

695

696

697

698

699

700

701

702



703  
704  
705  
706  
707  
708  
709  
710  
711  
712  
713  
714  
715  
716  
717  
718  
719  
720  
721  
722  
723  
724

**Table 5.** Statistical parameters of the QSPR-ANNoptimal model.

	Total phase	Training phase	Validation phase	Testing phase
$R^2$	0.9746	0.9710	0.9803	0.9872
RMSE	3.2466	3.4460	3.1136	2.2743
MAE	1.8235	1.8292	2.0710	1.5494
SEP	3.7747	4.0175	3.6540	2.5870
RER	28.5923	26.9384	29.1745	40.2866
RPD	628.1936	585.2833	701.7060	895.0705
MSE	10.5406	11.8746	9.6943	5.1724
MRSE	7.6634e-06	2.7226e-05	4.3237e-05	5.6940e-07
$A_f$	1.0064	1.0121	1.0152	1.0017
$B_f$	0.9936	0.9880	1.0152	0.9983

## Figures.

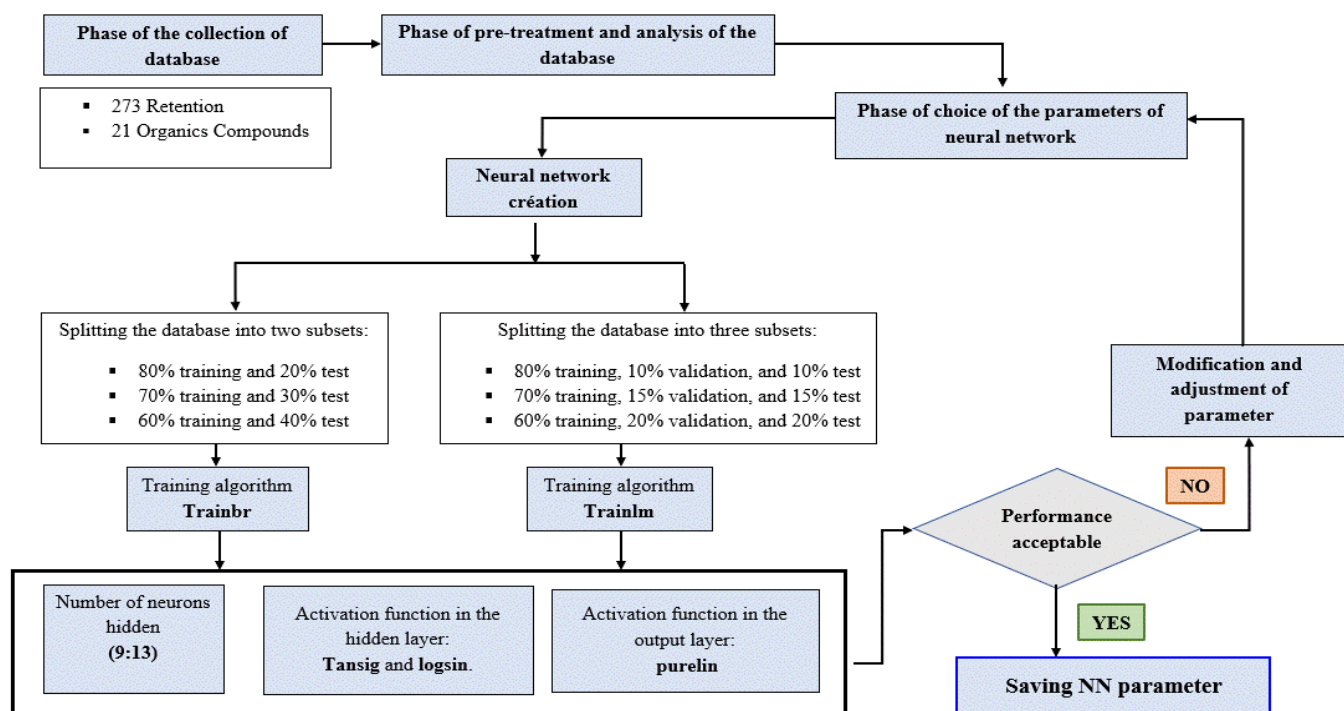
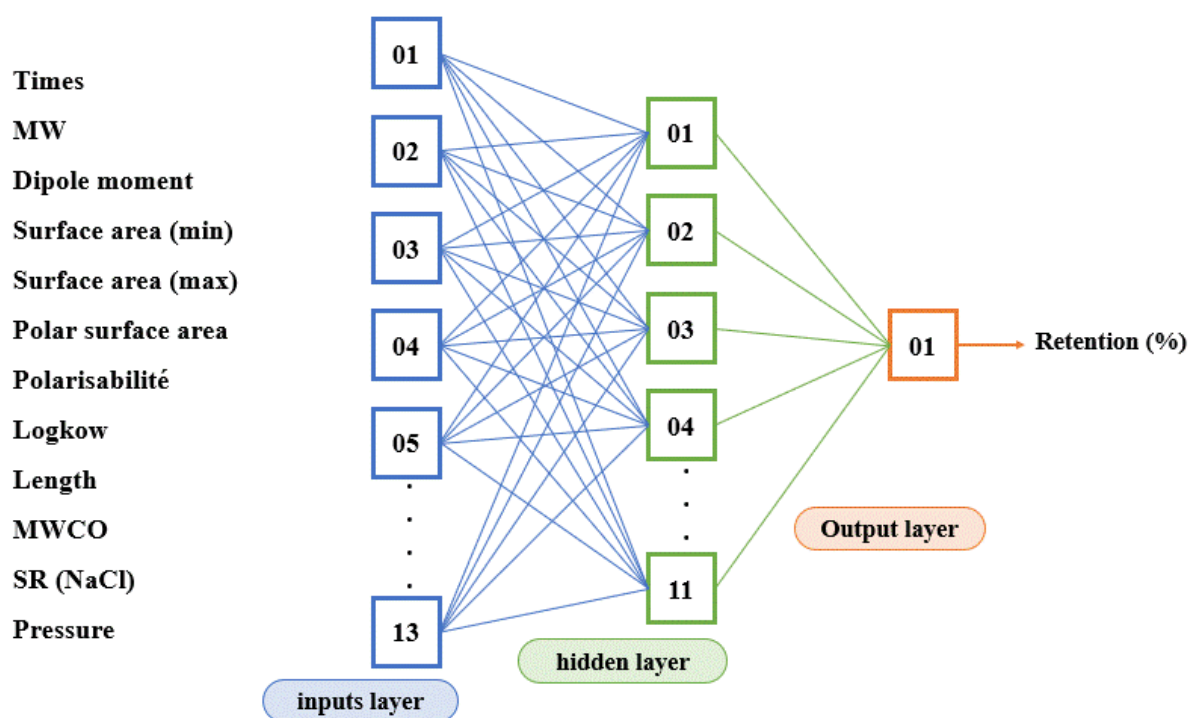
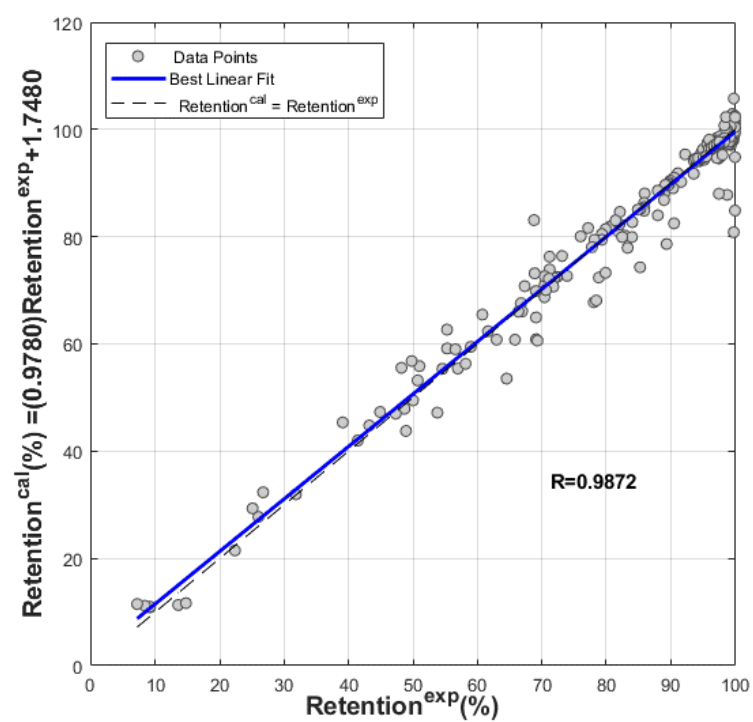


Figure 1. Designing the neural network architecture.

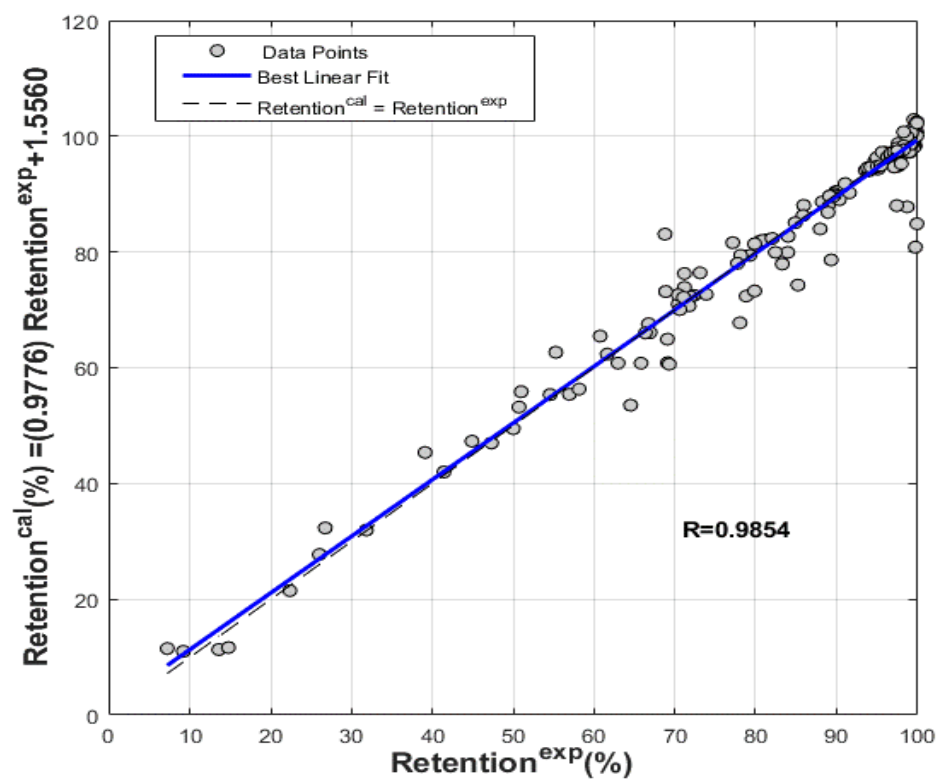
733



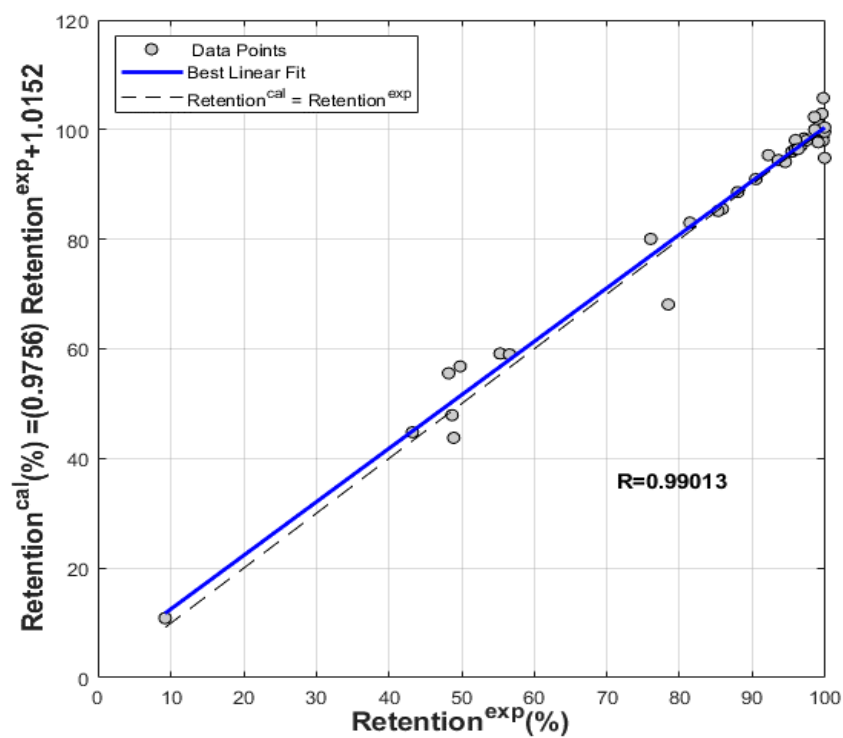
**Figure2.** Three-layer feed-forward neural network for modeling the



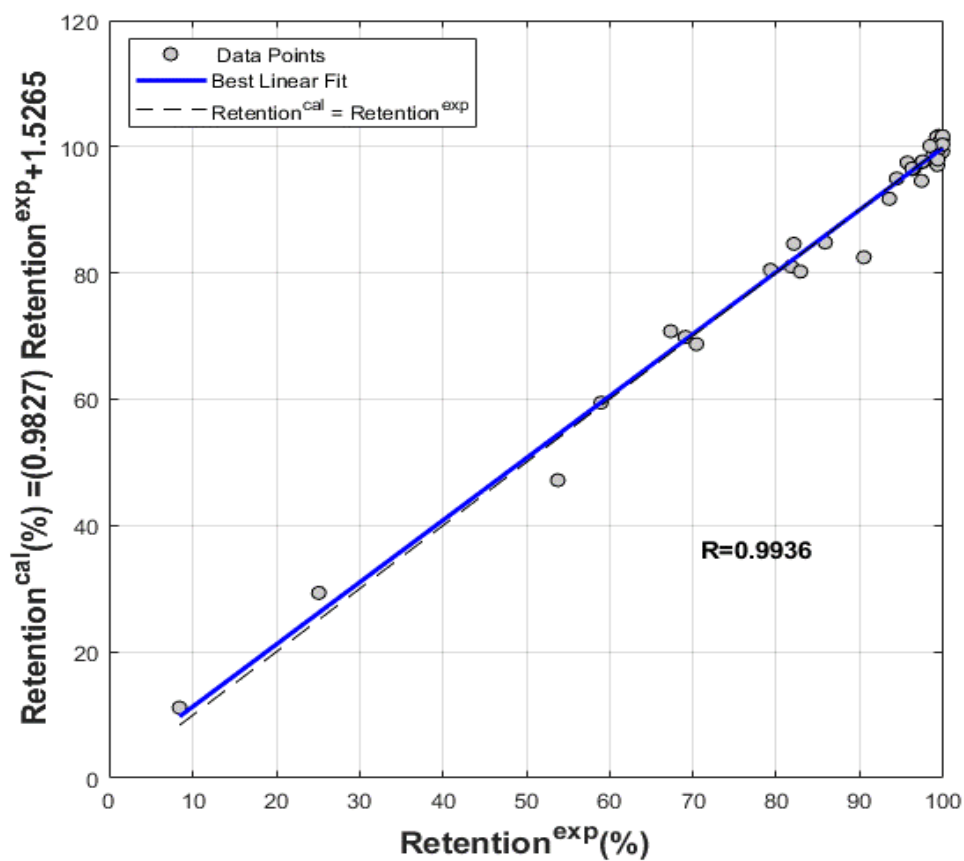
(a)



(b)



(c)



(d)

**Figures 3.** Comparison between experimental and calculated retention values for the total (a), training (b), validation (c), and testing phases (d).

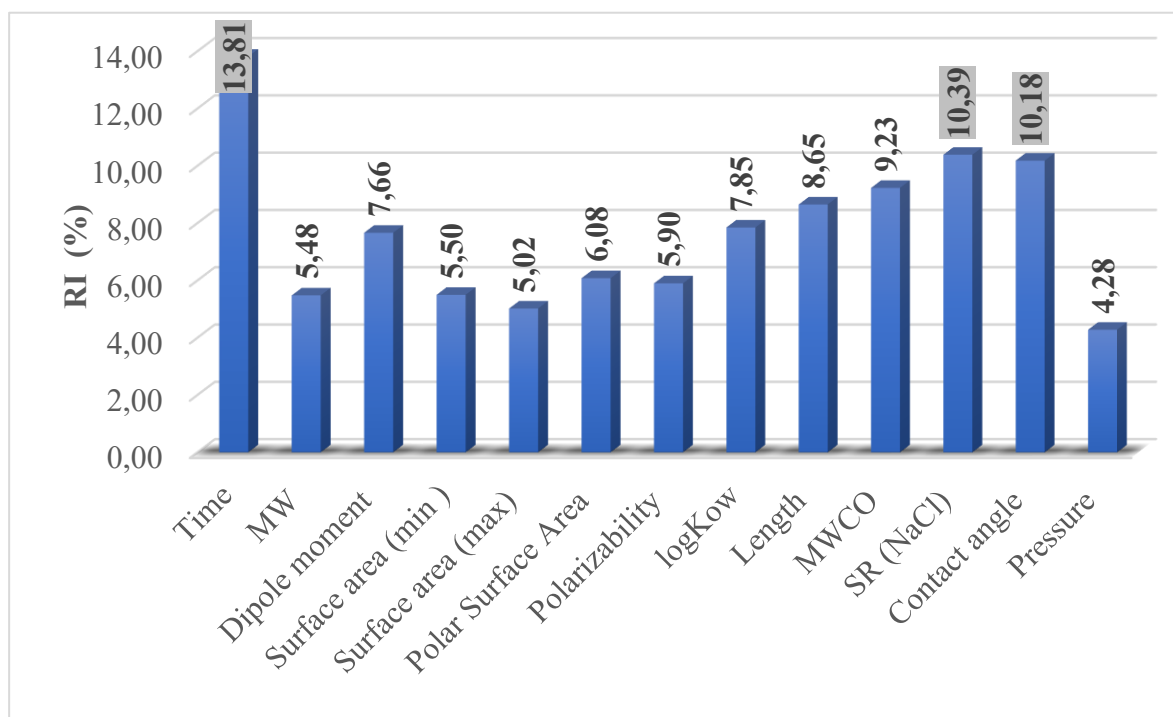


**Figure 4.** The histograms of the relative importance (RI) of the QSPR-ANN optimal for prediction of the effect of adsorption on the retention of OCs by RO/NF membranes.



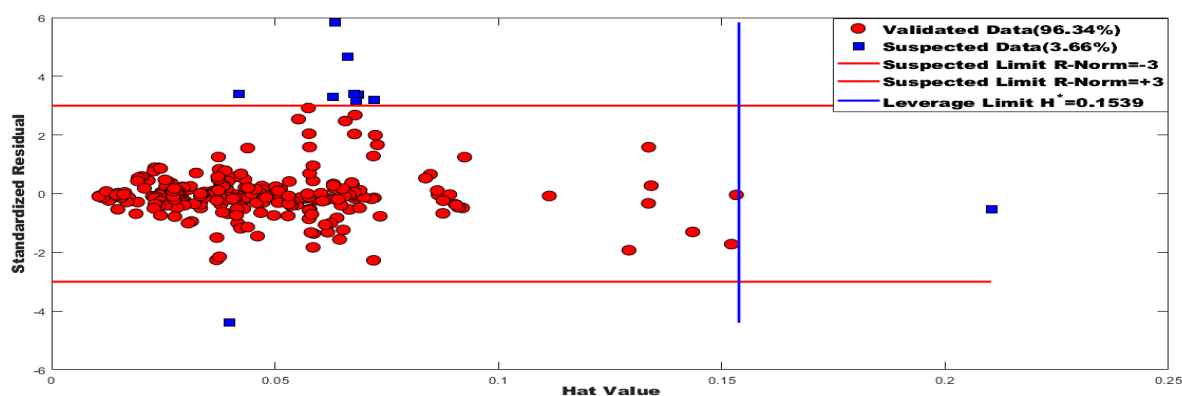


**Figure 5.** Williams range plot of QSPR-ANN optimal neural model for the total phase.

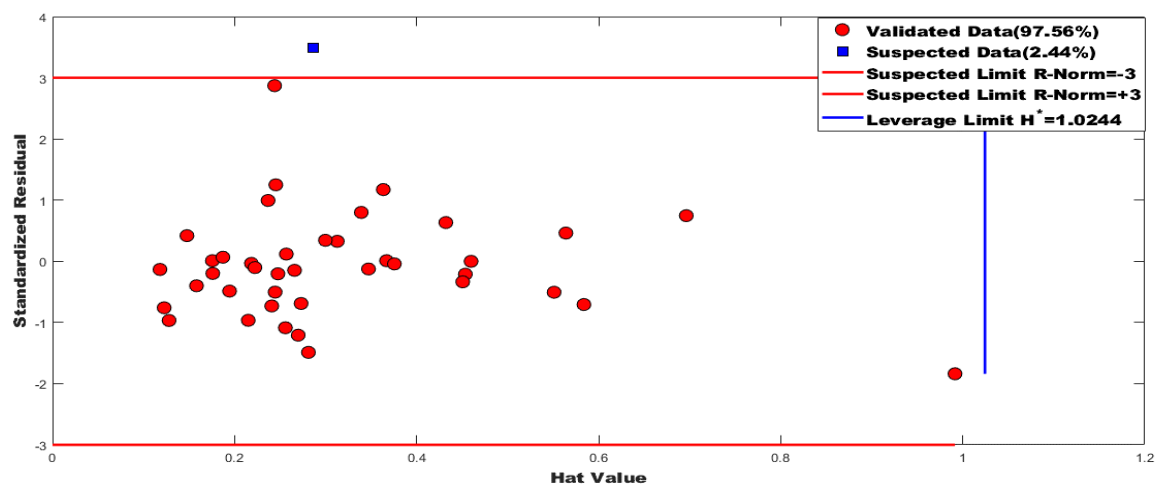


**Figure 6.** Williams range plot of QSPR-ANN optimal neural model for the testing phase.

## References

- Ammi, Y., Khaouane, L., & Hanini, S. (2015). Prediction of the rejection of organic compounds (neutral and ionic) by nanofiltration and reverse osmosis membranes using neural networks. *Korean Journal of Chemical Engineering*, 32(11), 2300–2310. <https://doi.org/10.1007/s11814-015-0086-y>
- Ammi, Y., Khaouane, L., & Hanini, S. (2018). A Model Based on Bootstrapped Neural Networks for Modeling the Removal of Organic Compounds by Nanofiltration and Reverse Osmosis Membranes. *Arabian Journal for Science and Engineering*, 43(11), 6271–6284. <https://doi.org/10.1007/s13369-018-3484-8>
- Ammi, Y., Khaouane, L., & Hanini, S. (2020). A Comparison of “Neural Networks and Multiple Linear Regressions” Models to Describe the Rejection of Micropollutants by Membranes. *Kemija u Industriji*, 69(3–4), 111–127. <https://doi.org/10.15255/kui.2019.024>
- Ammi, Y., Khaouane, L., & Hanini, S. (2021). Stacked neural networks for predicting the membranes performance by treating the pharmaceutical active compounds. *Neural Computing and Applications*, 33(19), 12429–12444. <https://doi.org/10.1007/s00521-021-05876-0>
- Ammi, Y., Moussa, C. S., & Hanini, S. (2023). Machine Learning and Neural Networks for Modelling the Retention of PPhACs by NF/RO. *Journal Kemija u Industriji*, 72, 11–12. <https://doi.org/10.21203/rs.3.rs-1120285/v1>
- Ammi, Y., Salah, H., & Latifa, K. (2021). an artificial intelligence approach for modeling the rejection of anti-inflammatory drugs by nanofiltration and reverse osmosis membranes using kernel support vector machine and neural networks. *Comptes Rendus - Chimie*, 24(2), 243–254. <https://doi.org/10.5802/crchim.76%3E>
- Arsuaga, J. M., López-Muñoz, M. J., & Sotto, A. (2010). Correlation between retention and adsorption of phenolic compounds in nanofiltration membranes. *Desalination*, 250(2), 829–832. <https://doi.org/10.1016/j.desal.2008.11.051>
- Baghban, A., Mohammadi, A. H., & Taleghani, M. S. (2017). Rigorous

- modeling of CO<sub>2</sub> equilibrium absorption in ionic liquids. *International Journal of Greenhouse Gas Control*, 58, 19–41.  
<https://doi.org/10.1016/j.ijggc.2016.12.009>
- Bellona, C., Drewes, J. E., Xu, P., & Amy, G. (2004). Factors affecting the rejection of organic solutes during NF/RO treatment - A literature review. *Water Research*, 38(12), 2795–2809.  
<https://doi.org/10.1016/j.watres.2004.03.034>
- Chan, M. K., Shams, A., Wang, C. C., Lee, P. Y., Jahani, Y., & Mirbagheri, S. A. (2023). Artificial Neural Network Model for Membrane Desalination: A Predictive and Optimization Study. *Computation*, 11(3). <https://doi.org/10.3390/computation11030068>
- Comerton, A. M., Andrews, R. C., Bagley, D. M., & Yang, P. (2007). Membrane adsorption of endocrine disrupting compounds and pharmaceutically active compounds. *Journal of Membrane Science*, 303(1–2), 267–277. <https://doi.org/10.1016/j.memsci.2007.07.025>
- Dahmani, A., Ammi, Y., & Hanini, S. (2022). *Neural network for prediction solar radiation in Relizane region ( Algeria ) - Analysis study*. 7(2), 8–18.
- Dolar, D., Drašinac, N., Košutić, K., Škorić, I., & Ašperger, D. (2017). Adsorption of hydrophilic and hydrophobic pharmaceuticals on RO/NF membranes: Identification of interactions using FTIR. *Journal of Applied Polymer Science*, 134(5), 17–21.  
<https://doi.org/10.1002/app.44426>
- Dolar, D., Košutić, K., & Ašperger, D. (2013). Influence of adsorption of pharmaceuticals onto RO/NF membranes on their removal from water. *Water, Air, and Soil Pollution*, 224(1). <https://doi.org/10.1007/s11270-012-1377-0>
- Fissa, M. R., Lahiouel, Y., Khaouane, L., & Hanini, S. (2023). Development of QSPR-ANN models for the estimation of critical properties of pure hydrocarbons. *Journal of Molecular Graphics and Modelling*, 121(108450).  
<https://doi.org/https://doi.org/10.1016/j.jmkgm.2023.108450>
- Gevrey, M., Dimopoulos, I., & Lek, S. (2003). Review and comparison of

- 947 methods to study the contribution of variables in artificial neural  
948 network models. *Ecological Modelling*, 160(3), 249–264.  
949 [https://doi.org/10.1016/S0304-3800\(02\)00257-0](https://doi.org/10.1016/S0304-3800(02)00257-0)
- 950 Gur-Reznik, S., Koren-Menashe, I., Heller-Grossman, L., Rufel, O., &  
951 Dosoretz, C. G. (2011). Influence of seasonal and operating conditions  
952 on the rejection of pharmaceutical active compounds by RO and NF  
953 membranes. *Desalination*, 277(1–3), 250–256.  
954 <https://doi.org/10.1016/j.desal.2011.04.029>
- 955 Hosseinzadeh, M., & Hemmati-Sarapardeh, A. (2014). Toward a predictive  
956 model for estimating viscosity of ternary mixtures containing ionic  
957 liquids. *Journal of Molecular Liquids*, 200(PB), 340–348.  
958 <https://doi.org/10.1016/j.molliq.2014.10.033>
- 959 Jawad, J., Hawari, A. H., & Javaid Zaidi, S. (2021). Artificial neural network  
960 modeling of wastewater treatment and desalination using membrane  
961 processes: A review. *Chemical Engineering Journal*, 419(June 2020),  
962 129540. <https://doi.org/10.1016/j.cej.2021.129540>
- 963 Khaouane, L., Ammi, Y., & Hanini, S. (2017). Modeling the Retention of  
964 Organic Compounds by Nanofiltration and Reverse Osmosis  
965 Membranes Using Bootstrap Aggregated Neural Networks. *Arabian  
966 Journal for Science and Engineering*, 42(4), 1443–1453.  
967 <https://doi.org/10.1007/s13369-016-2320-2>
- 968 Kim, S., Chu, K. H., Al-Hamadani, Y. A. J., Park, C. M., Jang, M., Kim, D.  
969 H., Yu, M., Heo, J., & Yoon, Y. (2018). Removal of contaminants of  
970 emerging concern by membranes in water and wastewater: A review.  
971 *Chemical Engineering Journal*, 335, 896–914.  
972 <https://doi.org/10.1016/j.cej.2017.11.044>
- 973 Kiso, Y., Sugiura, Y., Kitao, T., & Nishimura, K. (2001). Effects of  
974 hydrophobicity and molecular size on rejection of aromatic pesticides  
975 with nanofiltration membranes. *Journal of Membrane Science*, 192(1–  
976 2), 1–10. [https://doi.org/10.1016/S0376-7388\(01\)00411-2](https://doi.org/10.1016/S0376-7388(01)00411-2)
- 977 Kratbi, F., Ammi, Y., & Hanini, S. (2023). Support Vector Machines for  
978 Evaluating the Impact of the Forward Osmosis Membrane  
979 Characteristics on the Rejection of the Organic Molecules. *Kemija u*

980 *Industriji*, 72(7–8). <https://doi.org/10.15255/kui.2022.081>

981 Libotean, D., Giralt, J., Rallo, R., Cohen, Y., Giralt, F., Ridgway, H. F.,  
 982 Rodriguez, G., & Phipps, D. (2008). Organic compounds passage  
 983 through RO membranes. *Journal of Membrane Science*, 313(1–2), 23–  
 984 43. <https://doi.org/10.1016/j.memsci.2007.11.052>

985 Liu, Y. ling, Wang, X. mao, Yang, H. wei, & Xie, Y. F. (2018). Quantifying  
 986 the influence of solute-membrane interactions on adsorption and  
 987 rejection of pharmaceuticals by NF/RO membranes. *Journal of*  
 988 *Membrane Science*, 551(January), 37–46.  
 989 <https://doi.org/10.1016/j.memsci.2018.01.035>

990 Mahadeva, R., Kumar, M., Goel, A., Patole, S. P., & Manik, G. (2023). A  
 991 Novel AGPSO3-based ANN Prediction Approach: Application to the  
 992 RO Desalination Plant. *Arabian Journal for Science and Engineering*,  
 993 *April*. <https://doi.org/10.1007/s13369-023-07631-0>

994 Mahadeva, R., Mahendra, Kumar Shashikant P, P., & Manik, G. (2022).  
 995 Employing artificial neural network for accurate modeling, simulation  
 996 and performance analysis of an RO-based desalination process.  
 997 *Sustainable Computing: Informatics and Systems*, 35.  
 998 <https://doi.org/https://doi.org/10.1016/j.suscom.2022.100735>

999 Mohammad A, A., Soudan, B., Mahmoud, M. S., Sayed, E. T., AlMallahi,  
 1000 M. N., Inayat, A., Radi, M. Al, & Olabi, A. G. (2022). Progress of  
 1001 artificial neural networks applications in hydrogen production.  
 1002 *Chemical Engineering Research and Design*, 182, 66–86.  
 1003 <https://doi.org/https://doi.org/10.1016/j.cherd.2022.03.030>

1004 Mohammadi, A. H., Eslamimanesh, A., Gharagheizi, F., & Richon, D.  
 1005 (2012). A novel method for evaluation of asphaltene precipitation  
 1006 titration data. *Chemical Engineering Science*, 78, 181–185.  
 1007 <https://doi.org/10.1016/j.ces.2012.05.009>

1008 Peter J. Rousseeuw. (2005). *Outlier Diagnostics. Wiley Series in Probability*  
 1009 *and Statistics*. <https://doi.org/10.1002/0471725382.ch6>

1010 Rehab, I. A., Elsheikh, A. H., Mohamed Elasyed, A. E., & Mohammed A.A.,  
 1011 A. (2022). Chapter one - Basics of artificial neural networks. *Artificial*  
 1012 *Neural Networks for Renewable Energy Systems and Real-World*

Applications, 1–10. [https://doi.org/https://doi.org/10.1016/B978-0-12-820793-2.00002-1](https://doi.org/10.1016/B978-0-12-820793-2.00002-1)

Sediri, M., Hanini, S., Laidi, M., Turki, S. A., Cherifi, H., & Mabrouk, H. (2017). Artificial neural networks modeling of dynamic adsorption from aqueous solution. *Moroccan Journal of Chemistry*, 5(2), 2–5.

Shahmansouri, A., & Bellona, C. (2013). Application of quantitative structure-property relationships (QSPRs) to predict the rejection of organic solutes by nanofiltration. *Separation and Purification Technology*, 118, 627–638. <https://doi.org/10.1016/j.seppur.2013.07.050>

Teychene, B., Chi, F., Chokki, J., Darracq, G., Baron, J., Joyeux, M., & Gallard, H. (2020). Investigation of polar mobile organic compounds (PMOC) removal by reverse osmosis and nanofiltration: rejection mechanism modelling using decision tree. *Water Science and Technology: Water Supply*, 20(3), 975–983. <https://doi.org/10.2166/ws.2020.020>

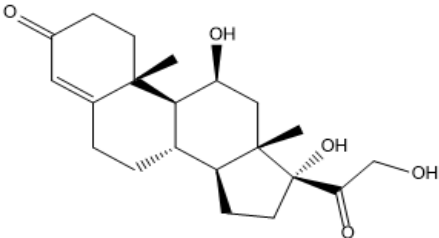
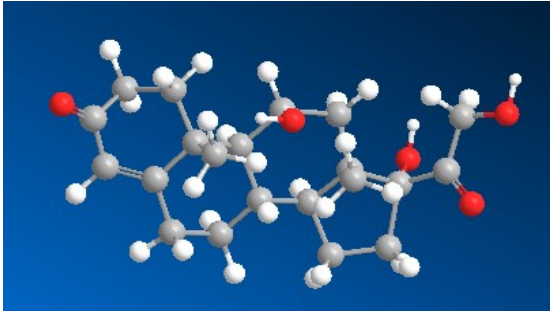
Viscarra Rossel, R. A., McGlynn, R. N., & McBratney, A. B. (2006). Determining the composition of mineral-organic mixes using UV-vis-NIR diffuse reflectance spectroscopy. *Geoderma*, 137(1–2), 70–82. <https://doi.org/10.1016/j.geoderma.2006.07.004>

Wang, R., Jiang, J., Pan, Y., Cao, H., & Cui, Y. (2009). Prediction of impact sensitivity of nitro energetic compounds by neural network based on electrotopological-state indices. *Journal of Hazardous Materials*, 166(1), 155–186. <https://doi.org/10.1016/j.jhazmat.2008.11.005>

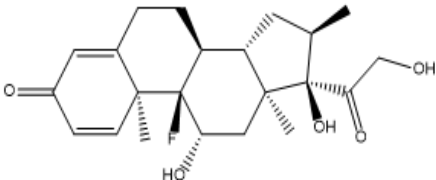
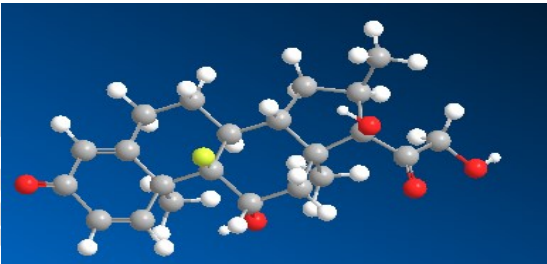
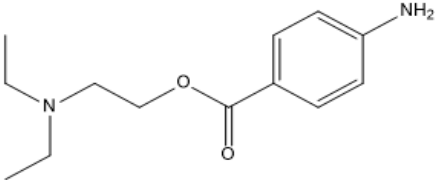

Yangali-Quintanilla, V., Verliefde, A., Kim, T. U., Sadmani, A., Kennedy, M., & Amy, G. (2009). Artificial neural network models based on QSAR for predicting rejection of neutral organic compounds by polyamide nanofiltration and reverse osmosis membranes. *Journal of Membrane Science*, 342(1–2), 251–262. <https://doi.org/10.1016/j.memsci.2009.06.048>.

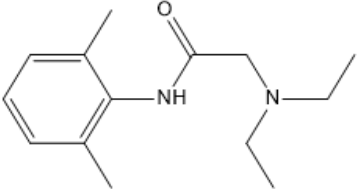
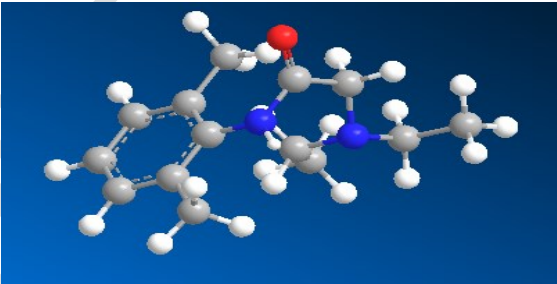
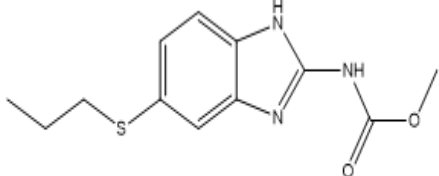

## Supplementary Data

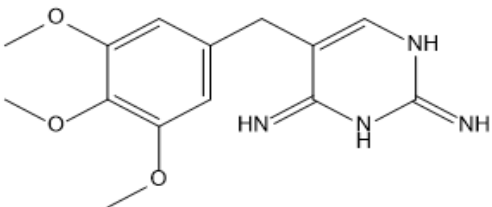
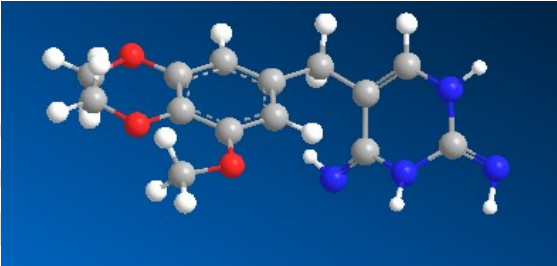
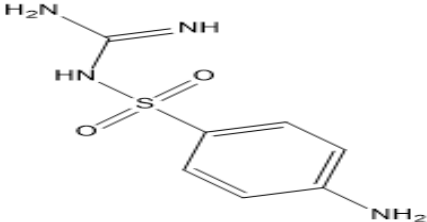
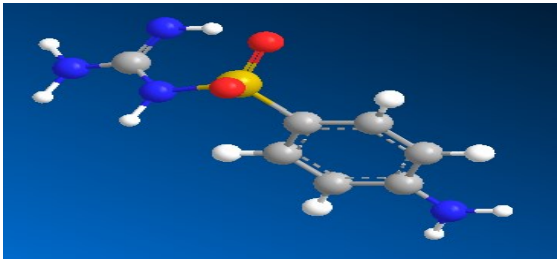
**Table 01.** The list of 21 Organic compounds

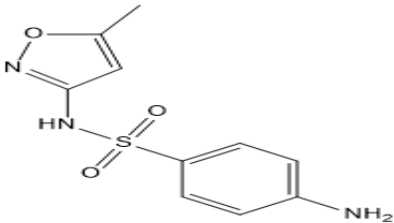
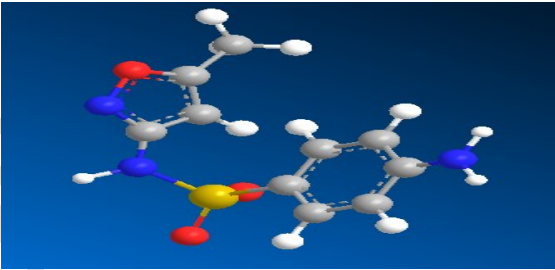
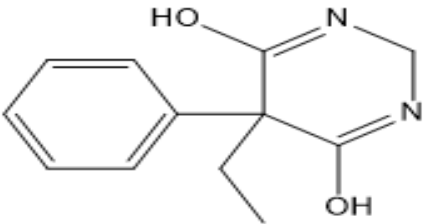
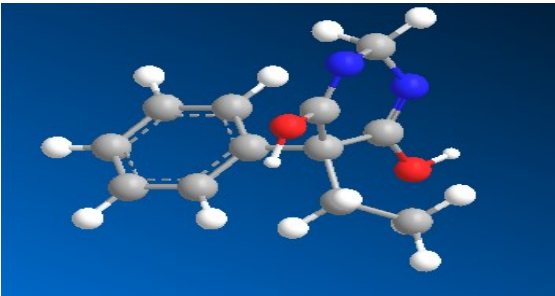
	Name	Mw (g/mol)	Formula 2D	Formula 3D
01	Hydrocortisone	362.47	 <p>The 2D chemical structure of Hydrocortisone is a steroid molecule. It features a four-ring core with a ketone group at C3, a double bond between C4 and C5, a hydroxyl group at C11, and a side chain at C17 consisting of a ketone group, a hydroxyl group, and a primary alcohol group.</p>	 <p>The 3D ball-and-stick model of Hydrocortisone shows the spatial arrangement of atoms. Carbon atoms are represented by grey spheres, hydrogen by white, oxygen by red, and the ketone and hydroxyl groups are clearly visible in their 3D orientation.</p>

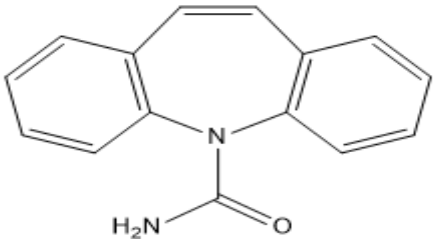
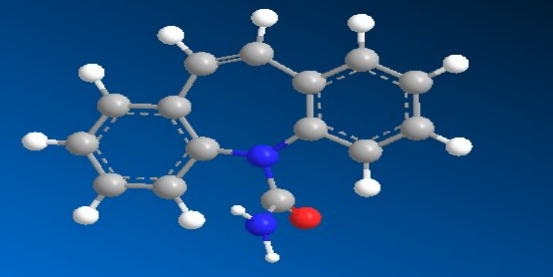
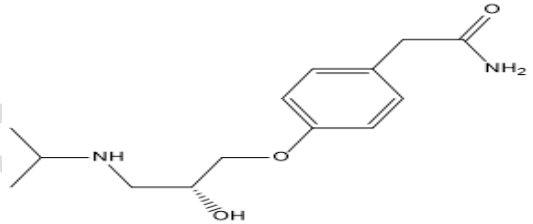
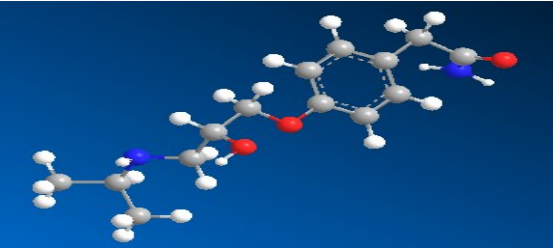


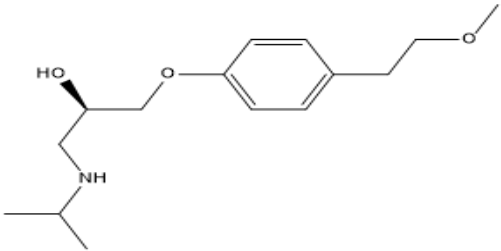
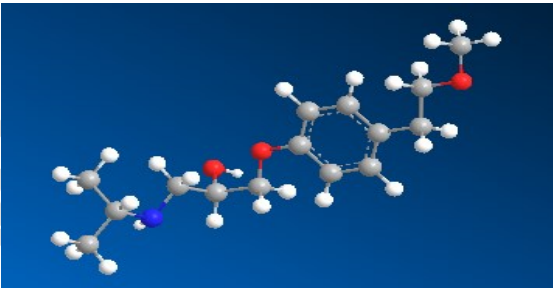
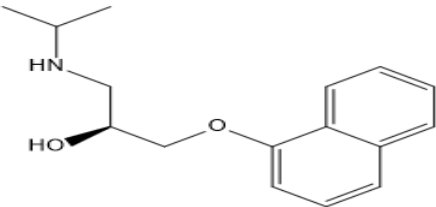
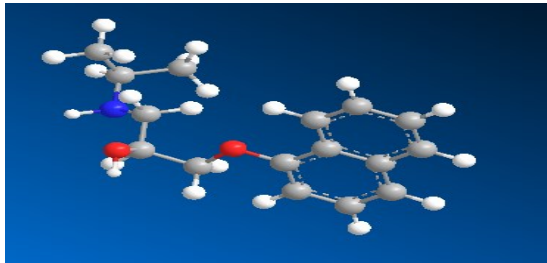
02	Dexaméthasone	392.47		
03	Procaine	236.32		

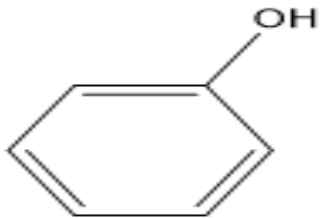
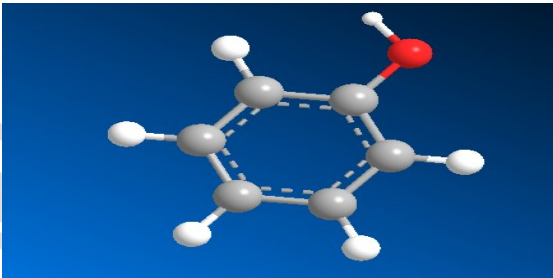
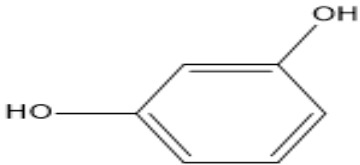
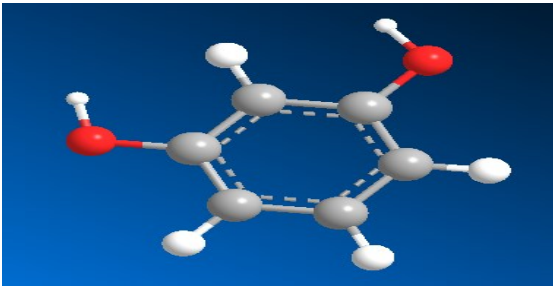
04	Lidocaine	234.34	 <chem>CCN(CC)CC(=O)Nc1ccccc1C</chem>	
05	Albendazole	265.33	 <chem>COC(=O)Nc1nc2cc(ccc2n1)SCCC</chem>	

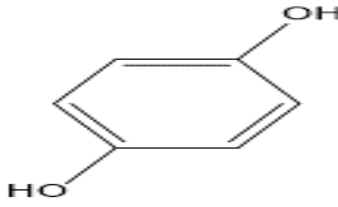
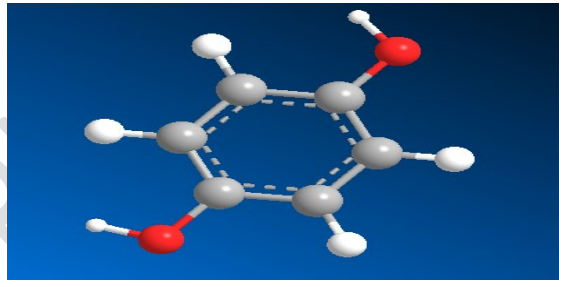
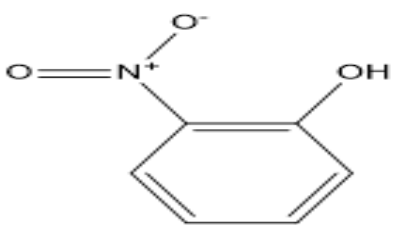
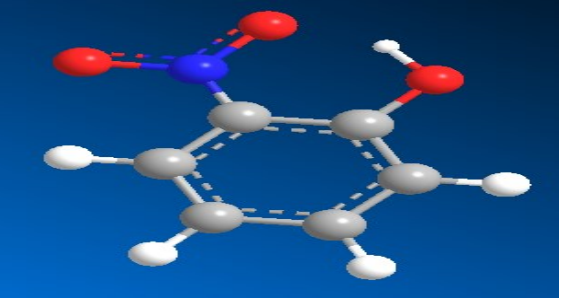
06	Trimethoprim	290.32		
07	Sulfaguanidine	214.24		

08	Sulfamethoxazole	253.3	 <p>Chemical structure of Sulfamethoxazole, showing a 5-methyl-4-isoxazole ring connected via a sulfonamide group to a 4-aminophenyl ring.</p>	 <p>3D ball-and-stick model of Sulfamethoxazole, showing the spatial arrangement of atoms (Carbon in grey, Nitrogen in blue, Oxygen in red, Sulfur in yellow, and Hydrogen in white).</p>
09	Primidone	218.1	 <p>Chemical structure of Primidone, showing a 2-ethyl-5-phenyl-2,4,6-trioxo-1,2,3,4-tetrahydropyrimidin-1(2H)-one ring system.</p>	 <p>3D ball-and-stick model of Primidone, showing the spatial arrangement of atoms (Carbon in grey, Nitrogen in blue, Oxygen in red, and Hydrogen in white).</p>

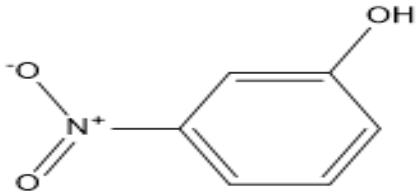
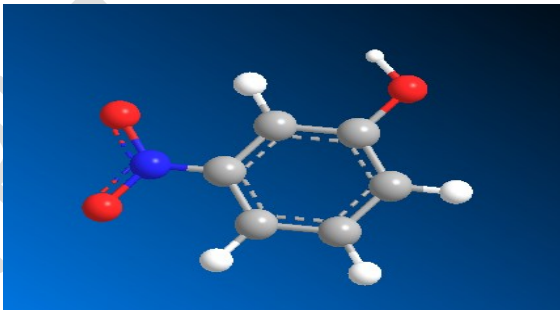
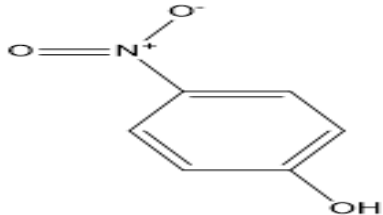
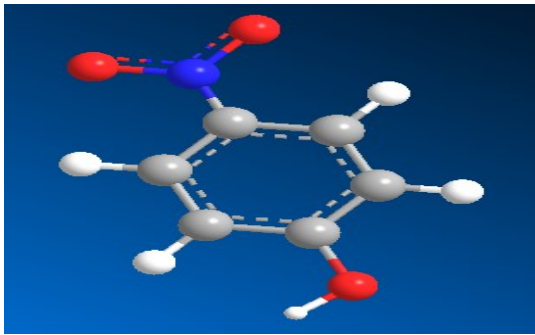
10	Carbamazepine	236.269	 <p>Chemical structure of Carbamazepine, showing a tricyclic system with a benzene ring fused to a seven-membered ring, which is further fused to another benzene ring. A carbonyl group (C=O) is attached to the seven-membered ring, and an amino group (H<sub>2</sub>N) is attached to the carbonyl carbon.</p>	 <p>3D ball-and-stick model of Carbamazepine, showing the spatial arrangement of atoms (carbon in grey, hydrogen in white, nitrogen in blue, and oxygen in red) and the overall molecular shape.</p>
11	Atenolol	266.3	 <p>Chemical structure of Atenolol, showing a benzene ring with a carboxamide group (C(=O)NH<sub>2</sub>) at the para position and a side chain at the other para position. The side chain consists of an ether linkage (-O-) connected to a chiral carbon atom (marked with a wedge bond to a hydroxyl group, -OH), which is further connected to a secondary amine group (-NH-) and an isopropyl group.</p>	 <p>3D ball-and-stick model of Atenolol, showing the spatial arrangement of atoms (carbon in grey, hydrogen in white, nitrogen in blue, and oxygen in red) and the overall molecular shape.</p>

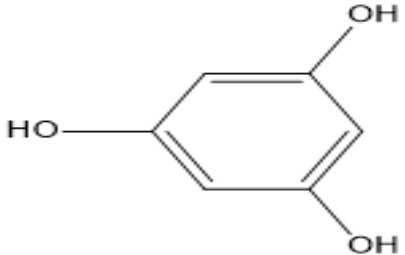
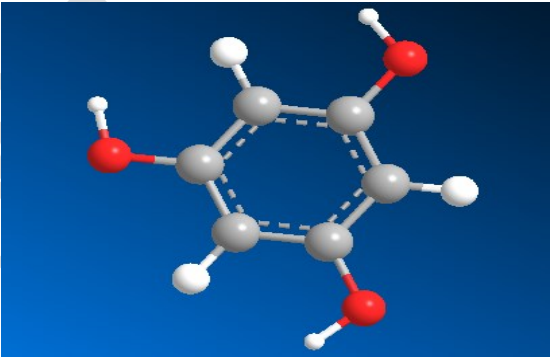
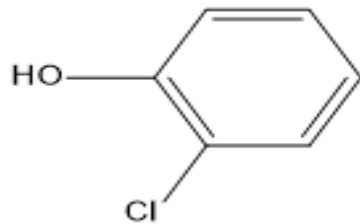
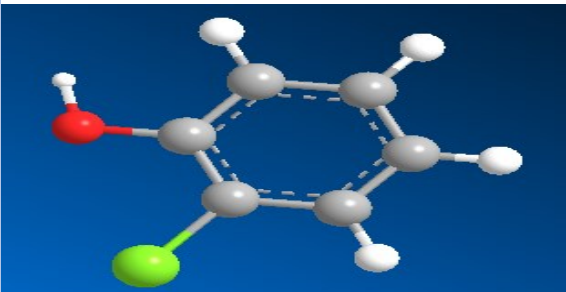
12	metoprolol	267.4	 <p>Chemical structure of metoprolol, showing a 1-methoxy-3-(isopropylamino)propan-2-ol moiety linked via an ether bridge to a 4-(2-methoxyethyl)phenyl group.</p>	 <p>3D ball-and-stick model of metoprolol, highlighting the spatial arrangement of atoms and the overall molecular shape.</p>
13	Propranolol	259.3	 <p>Chemical structure of Propranolol, showing a 1-isopropyl-3-(naphthalen-1-yloxy)propan-2-ol moiety.</p>	 <p>3D ball-and-stick model of Propranolol, illustrating the spatial arrangement of atoms and the overall molecular structure.</p>

14	Phenol	94.11		
15	Resorcinol	110.11		

16	Hydroquinone	110.11		
17	2-nitrophenol	139.11		



18	3-nitrophenol		 <p>Chemical structure of 3-nitrophenol (m-nitrophenol). It consists of a benzene ring with a hydroxyl group (-OH) at position 1 and a nitro group (-NO<sub>2</sub>) at position 3. The nitro group is shown with a positive charge on the nitrogen atom and a negative charge on one of the oxygen atoms.</p>	 <p>3D ball-and-stick model of 3-nitrophenol. The model shows the spatial arrangement of atoms: carbon (grey), oxygen (red), and hydrogen (white). The benzene ring is planar, and the nitro group is attached to the ring at the meta position relative to the hydroxyl group.</p>
19	4-nitrophenol		 <p>Chemical structure of 4-nitrophenol (p-nitrophenol). It consists of a benzene ring with a hydroxyl group (-OH) at position 1 and a nitro group (-NO<sub>2</sub>) at position 4. The nitro group is shown with a positive charge on the nitrogen atom and a negative charge on one of the oxygen atoms.</p>	 <p>3D ball-and-stick model of 4-nitrophenol. The model shows the spatial arrangement of atoms: carbon (grey), oxygen (red), and hydrogen (white). The benzene ring is planar, and the nitro group is attached to the ring at the para position relative to the hydroxyl group.</p>

20	Phloroglucinol	126.11		
21	2-chlorophenol	128.56		

1046 **Table 02.** Weights and bias of the optimized NN model.

$w_{ji}^l$													Bais	$w_{1j}^h$	Bais
Time	MW	Dipole moment	Surface area (min)	Surface area (max)	Polar Surface Area	Polariza-bility	logKow	Length	MWCO	SR (NaCl)	Contact angle	Pressure	$b_j^h$	Rejection (%)	$b_1^0$
1.597	0.010	1.019	0.179	0.635	1.164	-0.705	0.990	1.041	0.633	-0.839	0.382	0.467	0.797	1.092	0.480
1.443	-1.347	-0.844	0.324	-0.153	-0.186	0.082	-0.296	0.310	-0.727	-0.790	-0.588	1.289	0.067	-0.638	
1.335	-0.086	-0.579	0.431	-0.408	-0.175	-0.656	-0.499	-0.043	-0.249	0.118	-2.046	0.059	-1.887	0.071	
-1.587	0.926	0.699	0.346	-0.713	-0.713	-0.044	0.650	0.865	-0.641	-1.516	0.867	0.132	0.460	0.745	
0.698	-0.161	-1.047	0.349	-0.082	-0.463	1.186	-0.301	-0.079	1.744	-0.213	-1.319	0.038	-0.579	-0.067	
-0.704	0.025	1.575	-0.486	-1.003	-0.218	-0.432	1.582	-1.340	1.640	0.878	0.056	-0.200	-0.174	-0.768	
0.384	-0.045	0.349	0.121	-0.134	0.025	0.733	1.443	0.360	-0.447	1.061	-1.315	-0.036	0.065	0.796	
0.518	0.225	-0.097	0.759	0.281	1.153	-0.129	-0.401	1.389	0.764	1.207	-1.438	-0.593	0.499	-0.537	
3.662	2.740	0.591	0.655	-0.259	-0.196	-0.534	-0.060	-1.537	-0.693	-0.129	0.248	-0.323	-0.944	0.105	
-1.152	-0.069	-0.184	-1.729	-1.358	-0.969	0.505	-0.387	-1.890	0.432	-1.306	-0.330	1.031	0.451	-0.693	

1.223	0.344	0.534	0.410	0.294	1.079	-0.472	-0.796	0.580	-1.166	-2.441	-0.222	-0.303	0.354	-0.516	
-------	-------	-------	-------	-------	-------	--------	--------	-------	--------	--------	--------	--------	-------	--------	--

1047